# Verification of the AIRS and MLS ozone algorithms based on retrieved daytime and nighttime ozone

Wannan Wang[1,2,3], Tianhai Cheng[1], Ronald J. van der A[3], Jos de Laat[3], and Jason E. Williams[3]

[1]Aerospace Information Research Institute, Chinese Academy of Sciences, Beijing, 100094, China
[2]University of Chinese Academy of Sciences, Beijing, 100049, China
[3]Royal Netherlands Meteorological Institute (KNMI), De Bilt, 3730 AE, the Netherlands

*Correspondence to*: Tianhai Cheng (chength@radi.ac.cn)

**Abstract.** Ozone ($O_3$) plays a significant role in weather and climate on regional to global spatial scales. Most studies on the variability in the total column of $O_3$ (TCO) are typically analysed using daytime data. Based on knowledge of the chemistry and transport of $O_3$, significant deviations between daytime and nighttime $O_3$ are only expected either in the planetary boundary layer (PBL) or high in the stratosphere or mesosphere, having little effect on the TCO. Hence, we expect the daytime and nighttime TCO to be very similar. However, a detailed evaluation of satellite measurements of daytime and nighttime TCO is still lacking, despite the existence of long term records of both. Comparing daytime and nighttime TCOs thus provides a novel approach to verify the retrieval algorithms of for example the Atmospheric InfraRed Sounder (AIRS) and the Microwave Limb Sounder (MLS). In addition, such a comparison also helps in assessing the value of nighttime TCO for scientific research. Applying this verification on the AIRS and the MLS data we identified inconsistencies in observations of $O_3$ from both satellite instruments. For AIRS, daytime-nighttime differences were found over oceans resembling cloud cover patterns, and over land, mostly over dry land areas, likely related to infrared surface emissivity. These differences point to issues with the representation of both processes in the AIRS retrieval algorithm. For MLS, a major issue was identified with the "ascending-descending" orbit flag, used to discriminate nighttime and daytime MLS measurements. Disregarding this issue, MLS day-night differences were significantly smaller than AIRS day-night differences, providing additional support for retrieval method origin of AIRS day-night TCO differences. MLS day-night differences are dominated by the upper stratospheric and mesospheric diurnal $O_3$ cycle. These results provide useful information for improving infrared $O_3$ products and at the same time will allow study the day-night differences of stratospheric and mesospheric $O_3$.

## 1 Introduction

Atmospheric ozone ($O_3$) is a key factor in the structure and dynamics of the Earth's atmosphere (London 1980). The 1987 Montreal Protocol on Substances that Deplete the $O_3$ Layer formally recognized the significant threat of chlorofluorocarbons and other $O_3$-depleting substances (ODCs) to the $O_3$ layer and marks the start of joint international efforts to reduce and ultimately phase-out the global production and consumption of ODCs (Velders et al., 2007). Indeed, concerns about changes

30    in $O_3$ due to catalytic chemistry involving man-made chlorofluorocarbons has become an important topic for the scientific community, the general public and governments (Fioletov et al., 2002).

In response to this concern and associated environmental policies, during the last two decades a large number of studies have focused on estimating long-term variations and trends in stratospheric column of $O_3$ (SCO). A summary of the state of the science is frequently reported in the quadrennial $O_3$ Assessment Reports issued by the United Nations Environmental

35    Program (UNEP) and the World Meteorological Organization (WMO). These reports are written in response to the global treaties aiming at minimizing emissions of ODSs. The signatories of these treaties ask for regular updates on the state of the science and knowledge. The most recent $O_3$ Assessment reports extensively discuss long-term variations and trends in stratospheric $O_3$ in relation to expected recovery (WMO, 2011, 2014, 2018). According to WMO (2018), Antarctic stratospheric $O_3$ has started to recover, while outside of the polar regions, upper stratospheric $O_3$ has also increased. On the

40    other hand, no significant trend has been detected in global (60°S-60°N) total column $O_3$ over the 1997-2016 period with average values for the years since the last Assessment remaining roughly 2% below the 1964-1980 average. Moreover, recently a debate has emerged over the question as to whether lower stratospheric $O_3$ between 60°S-60°N has continued to decline despite decreasing $O_3$ depleting substances (Ball et al., 2018; Ball et al., 2019). In addition to the quadrennial $O_3$ Assessments, the Bulletin of the American Meteorological Society (BAMS) annually publishes its "State of the Climate", which since 2015

45    includes tropospheric $O_3$ trends and effects from El Nino-Southern Oscillation (ENSO) and a description of the relevant stratospheric events of the past year, the state of the Antarctic $O_3$ hole, as well as an annual update of global and zonal trends in stratospheric $O_3$. These regularly recurring reports and publications illustrate the continued attention and monitoring of the $O_3$ layer and its recovery, in which the long term records of satellite observations play a crucial role. Establishing and maintaining the quality of the satellite observations of stratospheric $O_3$ is therefore highly relevant.

50    A variety of techniques exist to measure the $O_3$ column and stratospheric $O_3$. UV absorption spectroscopy with the sun or stars as sources of UV light is the most used method to derive $O_3$ (Weeks et al., 1978; Fussen et al., 2000; Fu et al., 2013; Koukouli et al., 2015). In addition to the UV occultation method, the absorption of infrared radiation has also been used to detect $O_3$ profiles throughout the column (Gunson et al., 1990; Brühl et al., 1996). Another technique is the detection of the molecular oxygen dayglow emissions (Mlynczak and Drayson, 1990; Marsh et al., 2002). Some ground-based instruments use

55    $O_3$ emissions in the microwave region to infer the $O_3$ density in the mesosphere (Zommerfelds et al., 1989; Connor et al., 1994). Infrared emission measurements overcome the limitations in the local time coverage of solar occultation and dayglow technique and their altitude resolution is significantly higher compared with microwave measurements (Kaufmann et al., 2003). The strongest $O_3$ infrared absorption centres near 9.6 um.

Based on knowledge of chemistry and transport of $O_3$, significant deviations between daytime and nighttime $O_3$ are only

60    expected either in the planetary boundary layer (PBL) and high in the stratosphere or mesosphere, having little effect on the total column of $O_3$ (TCO). Hence, we expect that the daytime and nighttime TCO to be very similar. This slight variation in diurnal TCO can serve as a natural test signal for remote sensing instruments and data retrieval techniques. We need to clarify how sensitive different space-based instruments are to TCO slight changes and to distinguish potential biases from retrieval

artefacts. Day-night inter-comparisons present a unique opportunity to assess the internal consistency of infrared $O_3$
instruments (Brühl et al., 1996; Pommier et al., 2012; Parrish et al., 2014). Systematic differences could potentially arise, for
example, from temperature effects within the instrument, from differences in signal magnitude between daytime and nighttime
or from the retrieval algorithms. The Stratosphere Aerosol and Gas Experiment (SAGE) applied day-night differences to
validate $O_3$ profiles and found daytime values have a low bias due to errors in the retrieval method since the magnitude of the
difference was much less in a photochemical model (Cunnold et al., 1989). There are satellite instruments, like Atmospheric
InfraRed Sounder (AIRS) and The Microwave Limb Sounder (MLS), that provide global daytime and nighttime TCO/SCO
and $O_3$ profiles. Although their daytime $O_3$ retrievals have been validated (Livesey et al., 2008; Sitnov and Mokhov, 2016),
day-night differences in TCO and SCO are still largely unexplored. Applying this day-night verification on the AIRS and the
MLS data can assess their capacities to characterize atmospheric $O_3$. Furthermore, an accurate assessment of $O_3$ variation is
needed for a reliable and homogeneous long-term trend detection in the global $O_3$ distribution.

The $O_3$ diurnal cycle depends on latitude, altitude, weather and time. The variations of the diurnal cycle are less than 5%
in the tropics and subtropics and increase to more than 15% in the upper stratosphere during the polar day near 70 °N (Frith et
al., 2020). There exist diurnal variations in atmospheric $O_3$ at certain altitudes. There are two distinct $O_3$ maxima in the typical
vertical profile of the $O_3$ volume mixing ratio, one in the lower stratosphere and one in the mesosphere. The secondary
maximum in the mesosphere is present during both day and night (Evans and Llewellyn, 1972; Hays and Roble, 1973).
Chapman (1930) revealed the photochemical scheme in the mesosphere. The reactions of the Chapman cycle are important for
us to understand diurnal $O_3$ variation.

$$O_2 + hv \rightarrow 2O \, (\lambda < 240nm) \, , \tag{1}$$

$$O + O_2 + M \rightarrow O_3 + M, \text{ (in which M stands for an air molecule)} \tag{2}$$

$$O_3 + O \rightarrow 2O_2 \, , \tag{3}$$

$$O_3 + hv \rightarrow O_2 + O \, (\lambda < 1140nm) \, , \tag{4}$$
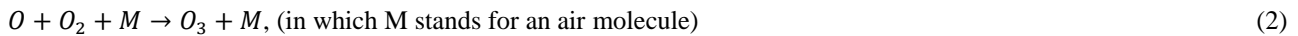
In the daytime mesosphere, catalytic $O_3$ depletion by odd hydrogen has to be considered in addition to the Chapman cycle.
The anti-correlation of $O_3$ and temperature is mainly due to the temperature dependence of the chemical rate coefficients (Craig
and Ohring, 1958; Barnett et al., 1975). Huang et al. (2008) and Huang et al. (1997) found midnight $O_3$ increases in the
mesosphere, based on SABER and MLS data, respectively. Zommerfelds et al. (1989) surmised that eddy transport may
explain this increase, while Connor et al. (1994) stated that atmospheric tides are expected to cause systematic day-night
variations.

During daytime, photolysis is the major loss process. The main nighttime $O_3$ source in the mesosphere is atomic oxygen,
while its sinks are atomic hydrogen and atomic oxygen (Smith and Marsh, 2005). In addition to $O_3$ chemical reactions with
active hydrogen and molecular, the turbulent mass transport also plays an important role in the explanation of the secondary
$O_3$ maximum (Sakazaki et al., 2013; Schanz et al., 2014).

Tropospheric $O_3$ is mainly produced during chemical reactions when mixtures of organic precursors ($CH_4$ and non-methane volatile organic carbon, NMVOC), CO, and nitrogen oxides (or $NO_x$), are exposed to the UV radiation in the troposphere (Simpson et al., 2014). At night, in the absence of the sunlight, there is no $O_3$ production, but surface $O_3$ deposition and dark reactions transform the $NO_x$-VOC mixture and remove $O_3$. The dark chemistry affects $O_3$ and its key ingredients mainly depend on the reactions of two nocturnal nitrogen oxides, $NO_3$ (the nitrate radical) and $N_2O_5$ (dinitrogen pentoxide). $NO_3$ oxidizes VOC at night, while reaction of $N_2O_5$ with aerosol particles containing water removes NOx. Both processes remove $O_3$ as well at night (Brown et al., 2006).

The diurnal cycle of $O_3$ in the middle stratosphere had generally been considered small enough to be inconsequential, with known larger variations in the upper stratosphere and mesosphere (Prather, 1981; Pallister and Tuck, 1983). Later studies have highlighted observed and modelled peak-to-peak variations of the order of 5% or more in the middle stratosphere between 30 and 1 hPa (Sakazaki et al., 2013; Parrish et al., 2014; Schanz et al., 2014).

In terms of dynamics, vertical transport due to atmospheric tides is expected to contribute to diurnal $O_3$ variations at altitudes where background $O_3$ levels have a sharp vertical gradient (Sakazaki et al., 2013). The Brewer/Dobson circulation transports air upwards in the tropics, polewards and downwards at high latitudes, with stronger transport towards the winter pole (Chipperfield et al., 2017).

The main objective of this paper is to analyse day-night differences in the AIRS TCO and the MLS SCO, as well as in MLS upper atmospheric $O_3$ profiles. Section 2 discusses the data used. Section 3 presents results for AIRS, MLS, the comparison of AIRS with MLS, and an application of AIRS TCO data over the Pacific low $O_3$ regions to highlight how day-night differences affect use and interpretation of TCO data. Finally, section 4 ends the paper with a brief summary and conclusions.

## 2 Data

### 2.1 AIRS total column of $O_3$ retrievals

The AIRS satellite instrument was the first in a new generation of high spectral resolution infrared sounder instruments flown aboard the National Aeronautics and Space Administration (NASA) Earth Observing System (EOS) Aqua satellite ( Aumann et al., 2003, 2020; Chahine et al., 2006; Divakarla et al., 2008). The AIRS radiance data at 9.6 μm band are used to retrieve column $O_3$ and $O_3$ profiles during both day and night (including the polar night) (Pittman et al., 2009; Fu et al., 2018; Susskind et al., 2003, 2011, 2014). The AIRS V6 level 3 daily standard physical retrieval products (2003-2018) provide TCO and profiles of retrieved $O_3$. The daily level 3 products comprise daily averaged measurements on the ascending and descending branches of an orbit with the quality indicators 'best' and 'good' and binned into 1 $°\times$1 $°$(latitude $\times$longitude) grid cells. The $O_3$ profile is vertically resolved in 28 levels between 1100 hPa and 0.1 hPa. This makes it possible to compare SCO between AIRS and MLS. Besides, estimates of the errors associated with cloud and surface properties is part of the AIRS V6 level 2 standard physical retrieval product, which we used here to discuss further details. Outside of the polar zones (60 $°$N-90 $°$N and

90 ˚S-60 ˚S), ascending and descending correspond respectively to daytime (13:30 in local solar time) and nighttime (01:30 in local solar time). Hereafter we refer to "day" and "night" rather than ascending and descending over 60°S-60 ˚N. In the polar zones, it is inappropriate to use ascending/descending mode to define daytime/nighttime, therefore, we just compare differences between ascending and descending mode. AIRS TCO measurements agree well with the global Brewer/Dobson Network station measurements with a bias of less than 4% and a root mean squared error (RMSE) difference of approximately 8% (Divakarla et al., 2008; Nalli et al., 2018; Smith and Barnet, 2019). Analysis of AIRS TCO monthly maps revealed that its retrievals depict seasonal trends and patterns in concurrence with OMI and SBUV/2 observations (Divakarla et al., 2008; Tian et al., 2007).

## 2.2 MLS stratospheric column of $O_3$ and $O_3$ profile retrievals

The MLS instrument on-board Aura satellite, which was launched on 15 July 2004 and placed into a near-polar Earth orbit at 705 km with an inclination of 98 ˚, uses the microwave limb sounding technique to measure vertical profiles of chemical constituents and dynamical tracers between the upper troposphere and the lower mesosphere (Waters et al., 2006). Its orbital ascending mode is at 13:42 (local solar time) and the orbital descending mode at 01:42 (local solar time) over 60 ˚S-60 ˚N. In this study, we use the MLS v4.2x standard $O_3$ product during 2005-2018. Its retrieval is using 240-GHz radiance, providing near-global spatial coverage (82 ˚S to 82 ˚N latitude), with each profile spaced 1.5 degrees or ~165 km along the orbit track. This $O_3$ product includes the $O_3$ profile on 55 pressure surfaces and the recommended useful vertical range is from 261 to 0.02 hPa. In addition, it contains an $O_3$ column, which is the integrated stratospheric column down to the thermal tropopause calculated from MLS measured temperature (Livesey et al., 2015). Jiang et al. (2007) found the MLS stratospheric $O_3$ data between 120 and 3 hPa agreed well with ozonesonde measurements, within 8% for the global daily average. Froidevaux et al. (2008) reported MLS stratospheric $O_3$ uncertainties of the order of 5%, with values closer to 10% (and occasionally 20%) at the lowest stratospheric altitudes. Livesey et al. (2008) estimated the MLS $O_3$ accuracy as ~40 ppbv ±5% (~20 ppbv ±20% at 215 hPa). Expectations and comparisons with other observations show good agreements for the MLS $O_3$ product, generally consistent with the systematic errors quoted above.

## 3 Results

### 3.1 AIRS $O_3$ retrievals day-night differences

Figure 1 shows spatial variations in the differences between the AIRS day and night measurements. Generally, 90% of the world's AIRS TCO is smaller during nighttime compared to daytime. The reduction of AIRS TCO over land at night is greater than over oceans depending on surface type. Seasonal averaged $O_3$ day-to-night relative difference shown in Figures 1a to 1d reveal that AIRS TCO day and night difference variations in Asia, Europe and North America during winter in the Northern Hemisphere (DJF) are smaller than during summer-time (JJA), in line with the efficiency of photochemical production between seasons in the Northern Hemisphere. The Sahara desert shows maximum difference value during winter-

time when there are large day-night temperature differences. The same phenomenon is observed in Western Australia during summer-time. The presence of day-night differences apparently correlating with surface infrared emissivity properties of dry desert regions is consistent with Masiello et al. (2014), who discussed the variability of surface infrared emissivity in the Sahara desert and recommended to take the diurnal variation of surface emissivity into account in infrared retrieval algorithms.

Figure 1e shows for the annual mean large differences of AIRS TCO retrievals over deserts, difference patterns over the oceans associated with the Intertropical Convergence Zone (ITCZ) as well as regions with persistent seasonal subtropical stratocumulus fields. The spatial patterns over land mimic regions with low IR surface emissivity and/or regions where IR surface emissivity exhibits large seasonal variations (Feltz et al., 2018). Figure 1f shows absolute differences between all subsequent pixels in the longitude direction. The figure reveals significant non-physical TCO changes (discontinuities) for adjacent land-ocean pixels (visible at coast lines running in North-South direction). All these effects are important parameters for the retrieval algorithm but bear no physical relation with total $O_3$. The observed diurnal cycle in AIRS TCO is related to either the measurements or to the algorithm. If the diurnal cycles in AIRS TCO are related to the retrieval algorithm, it has to be caused by the representation of a process in the algorithm having a diurnal cycle, something Smith and Barnes (2019) argue is not in the algorithm but should be taken into account. Hence, the differences shown in Figure 1 provide strong indications that the largest AIRS day-night TCO differences are dominated by retrieval artefacts. As such changes are unphysical, it confirms the hypothesis that clouds and the surface type (land/desert/vegetation/snow or ice) affects the AIRS TCO retrievals. Note that TCO day-night differences over land could also be (partly) related to clouds.

The AIRS emissivity retrieval uses the NOAA regression emissivity product as a first guess over land. The NOAA approach is based on clear radiances simulated from the European Centre for Medium-Range Weather Forecasts (ECMWF) forecast and a surface emissivity training data set (Goldberg et al., 2003). The training data set used for the AIRS V4 algorithm has a limited number of soil, ice, and snow types and very little emissivity variability in the training ensemble. In the AIRS V5 version, the regression coefficient set has been upgraded using a number of published emissivity spectra (12 spectra for ice/snow, 14 for land) blended randomly for land and ice (Zhou et al., 2008). These improvements generated a better emissivity first guess for use with the AIRS V5, and improved retrievals over the desert regions (Divakarla et al., 2008). In AIRS V6, a surface climatology was constructed from the 2008 monthly MODIS MYD11C3 emissivity product, and extended to the AIRS IR frequency hinge points using the baseline-fit approach described by Seemann et al. (2008). Note that AIRS observations with low information content (especially around the poles) will be drawn to the AIRS a-priori value. This AIRS a-priori for $O_3$ is a climatology without diurnal variation. If either the day or night observation has a lower information content than the other, this too can result in a day-night difference. This is probably the reason for the differences in Figure 1 over pole ice. Nevertheless, using day-night differences for evaluation of the AIRS V6 $O_3$ product suggest that further refinements for better surface emissivity retrievals are required and that issues related to cloud cover need to be solved.

## 3.2 MLS O$_3$ retrievals day-night differences

### 3.2.1 MLS O$_3$ profile

In order to better understand day-night differences in TCO, we also study day-night changes in the vertical profile of O$_3$ using MLS O$_3$ profile measurements. Figure 2a shows that the global (60°S-60°N) differences between day and night MLS O$_3$ profile occur in the mesosphere (10 hPa - 0.1 hPa). The O$_3$ mixing ratios are about an order of magnitude larger during night in the mesosphere, which was revealed by Huang et al. (2008) previously. Different latitude bands (30 degree) between 60°S and 60°N all display similar results.

We also find an unexpected polar bias at high latitudes in Figure 2d and 2g. On the one hand, the larger differences between ascending ("daytime") and descending ("nighttime") MLS O$_3$ profile at high latitude extend from the stratosphere to the mesosphere. On the other hand, ascending O$_3$ is smaller than descending O$_3$ at 10 hPa over 60°N-90°N in Figure 2d, which is in contrast with the result of other latitude bands.

### 3.2.2 MLS O$_3$ retrievals in 90°S-60°S and 60°N-90°N

The MLS O$_3$ profile polar bias mentioned above turns out to be related to an inconsistency in the 'AscDescMode' flag of MLS v4.2x standard O$_3$ product in 90°S-60°S and 60°N-90°N. We counted the daily number of pixels at both poles when observation mode is ascending (AscDescMode = 1) and descending (AscDescMode = -1) respectively. Figures 3a and 3c show there is a clear change on 14 May 2015 in the daily number of ascending/descending pixels, consistent with the change of MLS SCO in Figure 3b and 3d. Before 14 May 2015, there are very large differences (about 500 pixels, 95% of total pixels) in the number of pixels between ascending and descending mode, as well as the differences in MLS SCO. After 14 May 2015, the ascending and descending MLS SCO are much closer with smaller differences (about 20 pixels, 2% of total pixels) of ascending and descending pixels.

For the MLS O$_3$ profile in Figure 4, differences between ascending and descending MLS O$_3$ profiles at high latitudes for 2016-2018 are much smaller and more realistic compared to the differences for 2005-2014. The large differences in the stratosphere disappear in polar regions with the correct 'AscDescMode' flag for 2016-2018. For 60°N-90°N, ascending mode O$_3$ also becomes larger than descending mode O$_3$ at 10 hPa in Figure 4b. This indicates that the MLS 'AscDescMode' flag is correct for 2016-2018.

The O$_3$ retrieval algorithm adopted by the MLS v2.2 products has been validated to be highly accurate using multiple correlative measurements and the data have been used widely (Jiang et al., 2007; Froidevaux et al., 2008). The MLS v3.3 and v3.4, O$_3$ profile was reported on a finer vertical grid and the bottom pressure level with scientifically reliable values (MLS O$_3$ accuracy was estimated at ~20 ppbv +10% at 261 hPa) increases from 215 to 261 hPa (Livesey et al., 2015). The latest MLS v4.2x O$_3$ profile used in this study, released in February 2015, were in general similar to the previous version. One of the major improvements of MLS v4.2x was the handling of contamination from cloud signals in trace gas retrievals that resulted in significant reduction in the number of spurious MLS profile in cloudy regions and a more efficient screening of cloud-

contaminated measurements. Furthermore, the MLS O$_3$ products have been improved through additional retrieval phases and reduction in interferences from other species (Livesey et al., 2015). We find no indications that changes in instrument or algorithm are responsible for this 'AscDescMode' flag inconsistency. This flag inconsistency is not present between 60°S and 60 °N.

### 3.3 Comparison between AIRS and MLS O$_3$ retrievals

Figure 5 presents comparison of yearly and monthly averaged SCO for 2005-2018 observed by AIRS and MLS three latitude bands. Note that figure 5 is not meant as a validation of AIRS SCO with MLS SCO, but to explore the seasonality of either AIRS or MLS SCO day-night differences, and explore whether the seasonality in day-night SCO varies in unison over the seasons. Figure 5a shows the 14-year average daytime AIRS SCO (250 hPa – 1 hPa) and MLS SCO (261 hPa – 0.02 hPa) in 60 °S-60 °N for 2005-2018. The time average MLS SCO column is 260.62 DU and AIRS SCO is 264.24 DU. The average MLS SCO day-night differences for 2005-2018 (0.88 DU) is smaller than the AIRS SCO day-night differences observed for the same time period (5.24 DU). The day-night difference of MLS SCO is 0.79 DU in the mesosphere (10 hPa - 0.1 hPa) and 0.03 DU in the stratosphere (100 hPa - 10 hPa). The day-night difference of AIRS SCO is 1.51 DU in the mesosphere (10 hPa - 1 hPa) and 3.85 DU in the stratosphere (100 hPa - 10 hPa). Compared to the AIRS SCO day-night differences, the magnitude of MLS SCO day-night differences in the stratosphere and in the mesosphere are much smaller. It has been pointed out that errors in temperature profiles and water vapour mixing ratios will adversely affect the AIRS O$_3$ retrieval. Significant biases (0 - 100%) may exist in the region between ~300 hPa and ~80 hPa (Wang et al., 2019; Olsen et al., 2017). AIRS O$_3$ retrievals do not distinguish portions of the O$_3$ profile as being of different qualities, because all AIRS O$_3$ channels sense the surface as well atmospheric O$_3$. Thus AIRS O$_3$ retrievals are compromised if the surface is not well characterized (Olsen et al., 2017). In addition, AIRS SCO retrievals show smaller day-night differences in the polar zones (1-2 DU) than in 60 °S-60 °N (4-5 DU). This is related to clouds and the surface type which affect the AIRS O$_3$ retrievals as mentioned above. Figure 5b shows the monthly 14-year average daytime AIRS SCO and MLS SCO in the 60 °S-60 °N for 2005-2018. Seasonal or random changes of clouds and the surface emissivity have more significant impact on each monthly AIRS SCO retrieval than on the MLS SCO retrieval. Compared with the 60 °S-60 °N region, surface types in polar zones are less diverse (snow or ice). Therefore, the monthly 14-year average daytime AIRS SCO and MLS SCO in Figure 5d and 5f show similar patterns. Figures 5c to 5f also confirm that MLS SCO has a polar bias when compared with AIRS SCO at high latitudes. In addition, for MLS SCO in Figure 5f, the biggest day-night differences (50-60 DU) occur in September and October during the Antarctic O$_3$ hole.

### 3.4 Day-night difference of equatorial Pacific low O$_3$ regions

Generally, the Pacific low O$_3$ region (TCO < 220 DU) exist all year round and its size is larger at night than during the day, unlike the seasonal O$_3$ hole which occurs over Antarctica during the Southern Hemisphere polar winter. On the one hand, there are limited direct NO$_x$ emissions causing low O$_3$ over oceans compared to land. On the other hand, the low O$_3$ over the tropical western Pacific can be attributed to tropospheric O$_3$ loss in this area. Its presence is related to a pronounced minimum

in the tropospheric column of $O_3$ over the west Pacific, which loss is due to photochemical mechanism with higher air temperatures and higher water concentrations for $O_3$. In addition, high sea surface temperatures also favour strong convective activity in the tropical West Pacific, which can lead to low $O_3$ mixing ratios in the convective outflow regions in the upper troposphere in spite of the increased lifetime of odd oxygen (Kley et al., 1996; Rex et al., 2014). A further reduction in the tropospheric $O_3$ burden through bromine and iodine emitted from open-ocean marine sources has been postulated by numerical models (Vogt et al., 1999; von Glasow et al., 2002; von Glasow et al., 2004; Yang et al., 2005) and observations (Read et al., 2008).

Figure 6a and 6c show the low $O_3$ region is mainly located over the western Pacific by AIRS. Rajab et al. (2013) investigated similar low TCO in Malaysia using AIRS data. They found the highest $O_3$ concentration occurred in April and May and the lowest $O_3$ concentration occurred during November and December, which is consistent with our results in Figure 6f. They also found that $O_3$ concentrations exhibited an inverse relationship with rainfall, but was positively correlated with temperature. Figure 6b shows that besides in the tropical Western Pacific, low $O_3$ regions for MLS appear all over the tropical zone (30 °S-30 °N) at night. However, Figure 6d shows the occurrence frequency and intensity of daytime low $O_3$ regions by MLS SCO retrievals drastically reduces and exists mainly in tropical western Pacific. In Figure 6e and 6f, yearly and monthly averaged AIRS TCO and MLS SCO of the low $O_3$ regions show no consistency and regularity. The analysis of daytime MLS SCO of the low $O_3$ regions is based on only a few observations. We cannot distinguish whether it is an algorithm problem or a chemical mechanism that caused this phenomenon. For AIRS, clouds over oceans may have greater impact on the AIRS TCO retrievals at night. For MLS, more active chemical reactions may occur in these low $O_3$ regions at night.

For past, current and future monitoring of atmospheric phenomena like the Pacific tropospheric low $O_3$ area, it is important that observations are sufficient accurate. The evaluation of day-night differences in both MLS and AIRS has revealed the existence of biases in the satellite data that are sufficiently large in comparison to expected variations and changes in atmospheric $O_3$ that they may hamper the use of these satellite data studying them.

## 4 Conclusions

Comparison of daytime and nighttime AIRS TCO has revealed small but not insignificant biases in AIRS TCO. The differences are likely related to surface type (land/desert/vegetation/snow or ice) and infrared surface emissivity, especially over regions that exhibit smaller infrared emissivity or large seasonal variability in infrared emissivity. Differences typically were of the order of a few percent, which is significant given that long term changes in TCOs related to anthropogenic emissions of stratospheric $O_3$ depleting substances outside of polar regions are also of the order of a few percent.

Over land, patterns in day/night differences appear to be dominated by the dryness of the surface, suggesting that emissivity may not be well represented or that reduced sensitivity to the lower troposphere during night compared to day over hot surfaces results in a different AIRS TCO. The spatial inhomogeneity of day/night AIRS TCO differences over drier regions

285 points to emissivity dominating these differences. Infrared satellite retrieval artefacts due to land surface emissivity is well-known phenomenon (Zhou et al., 2013; George et al., 2015; Bauduin et al., 2017).

There were major changes to the surface emissivity retrieval in AIRS V6 compared to previous versions resulting in a very significant improvement in yield and accuracy for surface temperature and emissivity over land and ice surfaces compared to previous versions. Nevertheless, our results indicate that the AIRS V6 TCO still can be further improved with regard to the

290 representation of infrared emissivity. In addition, AIRS TCO differences over oceans bear a clear cloud cover signature which is likely related to uncertainties in the representation of clouds in the retrieval algorithm. The latter may also impact AIRS TCO retrievals over land, although detection of cloud features in AIRS TCO day-night differences over land is difficult due to the presence of the land surface emissivity related bias.

The strongest diurnal cycles in cloud fraction are found in the tropics over land, following strong daytime heating (Noel

295 et al., 2018). Over oceans, diurnal cycles in cloud fraction are weaker, but very broadly indicate reduced cloudiness during day compared to night, especially in the tropics and subtropics (Noel et al., 2018). In case of clouds, AIRS TCO appears to be larger during daytime compared to nighttime. This is consistent with the notion of increased cloudiness during the night, increasing the chance of shielding by undetected or unrecognized clouds in the AIRS retrieval. For ocean regions with persistent clouds during day and night (for example over ITCZ), Figure S1 in the supplement shows that variations of cloud

300 layer height have a greater impact on AIRS TCO day-night differences than of the cloud fraction.

Our results do not provide much evidence of another possible causes of day/night differences in AIRS TCO: the photochemical diurnal $O_3$ cycle in the lower troposphere and upper atmosphere. The strongest diurnal $O_3$ effects occur in the boundary layer over land due to nighttime surface deposition and daytime photochemical $O_3$ production in the presence of air pollution. In the marine boundary layer, the diurnal $O_3$ cycle is much weaker due to absence of air pollution and a general slow

305 $O_3$ destruction regime (~10%/day). Similarly, in the free troposphere, the diurnal $O_3$ cycle is also weak due to low $O_3$ production rates (generally low levels of pollution relevant for $O_3$ production). Hence, the diurnal $O_3$ cycle in the free troposphere above 750 hPa is negligible (Petetin et al., 2016). In summary, any tropospheric photochemical diurnal $O_3$ cycle effect should resemble some correspondence with air pollution. The day-night differences in AIRS TCO clearly do not resemble patterns of surface air pollution (Figure 1). MLS day/night differences are confined to the mesosphere (1 hPa and

310 higher). As shown in Smith et al. (2014) the lifetime of $O_3$ due to chemistry is strongly altitude dependent (< 20 min in the upper mesosphere above 0.01 hPa). Only in the mesosphere, the chemical lifetime of $O_3$ is long enough to see significant differences between average daytime and nighttime concentrations. However, the contribution of mesospheric $O_3$ to MLS SCO is negligible. The mesospheric diurnal $O_3$ cycle thus will also have a negligible effect on day/night AIRS TCO differences. In addition, Strode et al. (2019) simulated the global diurnal cycle in the tropospheric $O_3$ columns, their results indicated that the

315 mean peak-to-peak magnitude of the diurnal variability in tropospheric $O_3$ is approximately 1 DU. Figures S2 to S5 in the supplement also show that the AIRS TCO retrieval artefacts dominate the day/night variability of tropospheric $O_3$ residuals (TOR = AIRS TCO – MLS SCO).

In summary, our analysis has identified evidence and indications that clouds, land surface infrared emissivity, and sensitivity of satellite measurements to the lower troposphere, influence AIRS satellite TCO observations, pinpointing to areas and processes for algorithm improvement.

The MLS v4.2x was very useful for verification of daytime and nighttime SCO and $O_3$ profile between 60 °S-60 °N. MLS day-night differences in SCO and $O_3$ profiles show that day-night differences are only small (< 1 DU) and likely to be in the upper stratosphere and mesosphere. However, an inconsistency was found in the 'AscDescMode' flag in 60°N-90 °N and in 90 °S-60 °S, resulting in inconsistent profiles in these regions before 14 May 2015. In processor version v4.22 and later versions this issue has been fixed, but since it is a relatively small issue, the MLS data set before 2016 has not been reprocessed.

A case study of day-night differences $O_3$ over equatorial Pacific revealed that both AIRS and MLS $O_3$ retrievals have biases in comparison to expected variations and changes. Our results show that maintaining the quality of the satellite observations of stratospheric $O_3$ is therefore highly relevant.

**Data availability**

Satellite data sets used in this research can be requested from public sources. AIRS level 3 data are available online: AIRS Science Team/Joao Teixeira (2013), AIRS/Aqua L3 Daily Standard Physical Retrieval (AIRS-only) 1 degree x 1 degree V006, Greenbelt, MD, USA, Goddard Earth Sciences Data and Information Services Center (GES DISC), Accessed: [*2020.04*], doi:10.5067/Aqua/AIRS/DATA303.

AIRS level 2 data are available from: AIRS Science Team/Joao Teixeira (2013), AIRS/Aqua L2 Standard Physical Retrieval (AIRS-only) V006, Greenbelt, MD, USA, Goddard Earth Sciences Data and Information Services Center (GES DISC), Accessed: [*2020.04*], 10.5067/Aqua/AIRS/DATA202.

MLS level 2 data can be obtained from: Schwartz, M., Froidevaux, L., Livesey, N. and Read, W. (2015), MLS/Aura Level 2 Ozone (O3) Mixing Ratio V004, Greenbelt, MD, USA, Goddard Earth Sciences Data and Information Services Center (GES DISC), Accessed: [*2020.04*], doi:10.5067/Aura/MLS/DATA2017.

**Author contributions**

WNW and JL provided satellite data, tools, and analysis. RA, JL and THC undertook the conceptualization and investigation. WNW prepared original draft. RA and JL carried out review and editing. JW checked the English language. All authors discussed the results and commented on the paper.

**Competing interests**

The authors declare that they have no conflict of interest.

## Acknowledgements

The support provided by China Scholarship Council (CSC) during a visit of Wannan Wang to the Royal Netherlands Meteorological Institute (KNMI) is acknowledged.

## References

350 American Meteorological Society: https://www.ametsoc.org/index.cfm/ams/publications/bulletin-of-the-american-meteorological-society-bams/state-of-the-climate/, access: April 13 2020.

Aumann, H. H., Chahine, M. T., Gautier, C., Goldberg, M. D., Kalnay, E., McMillin, L. M., Revercomb, H., Rosenkranz, P. W., Smith, W. L., Staelin, D. H., Strow, L. L. and Susskind, J.: AIRS/AMSU/HSB on the aqua mission: design, science objectives, data products, and processing systems, IEEE Trans. Geosci. Remote Sens., 41(2), 253–264, 355 doi:10.1109/TGRS.2002.808356, 2003.

Aumann, H. H., Broberg, S. E., Manning, E. M., Pagano, T. S. and Wilson, R. C.: Evaluating the Absolute Calibration Accuracy and Stability of AIRS Using the CMC SST, Remote Sens., 12(17), 2743, doi:10.3390/rs12172743, 2020.

Ball, W. T., Alsing, J., Mortlock, D. J., Staehelin, J., Haigh, J. D., Peter, T., Tummon, F., St übi, R., Stenke, A., Anderson, J., Bourassa, A., Davis, S. M., Degenstein, D., Frith, S., Froidevaux, L., Roth, C., Sofieva, V., Wang, R., Wild, J., Yu, P., Ziemke, 360 J. R., and Rozanov, E. V.: Evidence for a continuous decline in lower stratospheric ozone offsetting ozone layer recovery, Atmos. Chem. Phys., 18, 1379–1394, https://doi.org/10.5194/acp-18-1379-2018, 2018.

Ball, W. T., Alsing, J., Staehelin, J., Davis, S. M., Froidevaux, L., and Peter, T.: Stratospheric ozone trends for 1985–2018: sensitivity to recent large variability, Atmos. Chem. Phys., 19, 12731–12748, https://doi.org/10.5194/acp-19-12731-2019, 2019.

365 Barnett, J.J., Houghton, J.T. and Pyle, J.A.: The temperature dependence of the ozone concentration near the stratopause. Q.J.R. Meteorol. Soc., 101: 245-257, https://doi.org/10.1002/qj.49710142808, 1975.

Bauduin, S., Clarisse, L., Theunissen, M., George, M., Hurtmans, D., Clerbaux, C., and Coheur, P.-F.: IASI's sensitivity to near-surface carbon monoxide (CO): Theoretical analyses and retrievals on test cases, Journal of Quantitative Spectroscopy and Radiative Transfer, 189, 428-440, https://doi.org/10.1016/j.jqsrt.2016.12.022, 2017.

370 Brown, S. S., Neuman, J. A., Ryerson, T. B., Trainer, M., Dube, W. P., Holloway, J. S., Warneke, C., de Gouw, J. A., Donnelly, S. G., Atlas, E., Matthew, B., Middlebrook, A. M., Peltier, R., Weber, R. J., Stohl, A., Meagher, J. F., Fehsenfeld, F. C., and Ravishankara, A. R.: Nocturnal odd-oxygen budget and its implications for ozone loss in the lower troposphere, Geophys Res Lett, 33, doi:10.1029/2006GL025900, 2006.

Br ühl, C., Drayson, S. R., Russell, J. M., Crutzen, P. J., McInerney, J. M., Purcell, P. N., Claude, H., Gernandt, H., McGee, T. 375 J., and McDermid, I. S.: Halogen Occultation Experiment ozone channel validation, J. Geophys. Res., 101( D6), 10217– 10240, doi:10.1029/95JD02031, 1996.

Chahine, M. T., Pagano, T. S., Aumann, H. H., Atlas, R., Barnet, C., Blaisdell, J., Chen, L., Divakarla, M., Fetzer, E. J., Goldberg, M., Gautier, C., Granger, S., Hannon, S., Irion, F. W., Kakar, R., Kalnay, E., Lambrigtsen, B. H., Lee, S.-Y., Le MARSHALL, J., Mcmillan, W. W., Mcmillin, L., Olsen, E. T., Revercomb, H., Rosenkranz, P., Smith, W. L., Staelin, D., 380 Strow, L. L., Susskind, J., Tobin, D., Wolf, W. and Zhou, L.: AIRS: Improving Weather Forecasting and Providing New Data on Greenhouse Gases, Bull. Am. Meteorol. Soc., 87(7), 911–926, doi:10.1175/BAMS-87-7-911, 2006.

Chapman, S.: A theory of upperatmospheric ozone, Mem. Roy. Meteor., 3, 103-125, 1930.

Chipperfield, M. P., Bekki, S., Dhomse, S., Harris, N. R. P., Hassler, B., Hossaini, R., Steinbrecht, W., Thieblemont, R., and Weber, M.: Detecting recovery of the stratospheric ozone layer, Nature, 549, 211-218, https://doi.org/10.1038/nature23681, 2017.

Connor, B. J., Siskind, D. E., Tsou, J., Parrish, A., and Remsberg, E. E.: Ground-based microwave observations of ozone in the upper stratosphere and mesosphere, J. Geophys. Res., 99( D8), 16757– 16770, doi:10.1029/94JD01153, 1994.

Craig, R. A., and Ohring, G.: The temperature dependence of ozone radiational heating rates in the vicinity of the mesopeak, J. Meteor., **15**, 59–62, https://doi.org/10.1175/1520-0469(1958)015<0059:TTDOOR>2.0.CO;2, 1958.

Cunnold, D., Chu, W., Barnes, R., McCormick, M., and Veiga, R.: Validation of SAGE II ozone measurements, J. Geophys. Res., 94(D6), 8447– 8460, doi:10.1029/JD094iD06p08447, 1989.

Divakarla, M., Barnet, C., Goldberg, M., Maddy, E., Irion, F., Newchurch, M., Liu, X. P., Wolf, W., Flynn, L., Labow, G., Xiong, X. Z., Wei, J., and Zhou, L. H.: Evaluation of Atmospheric Infrared Sounder ozone profiles and total ozone retrievals with matched ozonesonde measurements, ECMWF ozone data, and Ozone Monitoring Instrument retrievals, J. Geophys. Res., 113, D15308, doi:10.1029/2007JD009317, 2008.

Evans, W., and Llewellyn, E.: Measurements of mesospheric ozone from observations of the 1.27 μm band, Radio Science, 7, 45-50, doi: 10.1029/RS007i001p00045, 1972.

Feltz, M., Borbas, E., Knuteson, R., Hulley, G., and Hook, S.: The Combined ASTER and MODIS Emissivity over Land (CAMEL) Global Broadband Infrared Emissivity Product, Remote Sens., 10(7), 1027, https://doi.org/10.3390/rs10071027, 2018.

Fioletov, V. E., Bodeker, G. E., Miller, A. J., McPeters, R. D., and Stolarski, R.: Global and zonal total ozone variations estimated from ground-based and satellite measurements: 1964-2000, J. Geophys. Res., 107(D22), 4647, doi:10.1029/2001JD001350, 2002.

Frith, S. M., Bhartia, P. K., Oman, L. D., Kramarova, N. A., McPeters, R. D., and Labow, G. J.: Model-based climatology of diurnal variability in stratospheric ozone as a data analysis tool, Atmos. Meas. Tech., 13, 2733–2749, https://doi.org/10.5194/amt-13-2733-2020, 2020.

Froidevaux, L., Jiang, Y. B, Lambert, A., Livesey, N. J., Read, W. G., Waters, J. W., Browell, E. V., Hair, J. W., Avery, M. A., and McGee, T. J., Twigg, L. W., Sumnicht, G. K., Jucks, K. W., Margitan, J. J., Sen, B., Stachnik, R. A., Toon, G. C., Bernath, P. F., Boone, C. D., Walker, K. A., Filipiak, M. J., Harwood, R. S., Fuller, R. A., Manney, G. L., Schwartz, M. J., Daffer, W. H., Drouin, B. J., Cofield, R. E., Cuddy, D. T., Jarnot, R. F., Knosp, B. W., Perun, V. S., Snyder, W. V., Stek, P. C., Thurstans, R. P., and Wagner, P. A.: Validation of aura microwave limb sounder stratospheric ozone measurements, J. Geophys. Res., 113, D15S20, doi:10.1029/2007JD008771, 2008.

Fu, D., Worden, J. R., Liu, X., Kulawik, S. S., Bowman, K. W., and Natraj, V.: Characterization of ozone profiles derived from Aura TES and OMI radiances, Atmos. Chem. Phys., 13, 3445–3462, https://doi.org/10.5194/acp-13-3445-2013, 2013.

Fu, D., Kulawik, S. S., Miyazaki, K., Bowman, K. W., Worden, J. R., Eldering, A., Livesey, N. J., Teixeira, J., Irion, F. W., Herman, R. L., Osterman, G. B., Liu, X., Levelt, P. F., Thompson, A. M., and Luo, M.: Retrievals of tropospheric ozone profiles from the synergism of AIRS and OMI: methodology and validation, Atmos. Meas. Tech., 11, 5587–5605, https://doi.org/10.5194/amt-11-5587-2018, 2018.

Fussen, D., Vanhellemont, F., Bingen, C., and Chabrillat, S.: Ozone profiles from 30 to 110 km Measured by the Occultation Radiometer Instrument during the period Aug. 1992–Apr. 1993, Geophys Res Lett, 27, 3449-3452, https://doi.org/10.1029/2000GL011575, 2000.

George, M., Clerbaux, C., Bouarar, I., Coheur, P.-F., Deeter, M. N., Edwards, D. P., Francis, G., Gille, J. C., Hadji-Lazaro, J., Hurtmans, D., Inness, A., Mao, D., and Worden, H. M.: An examination of the long-term CO records from MOPITT and IASI: comparison of retrieval methodology, Atmos. Meas. Tech., 8, 4313–4328, https://doi.org/10.5194/amt-8-4313-2015, 2015.

425     Goldberg, M. D., Qu, Y., McMillin, L. M., Wolf, W., Zhou, L., and Divakarla, M.: AIRS near-real-time products and algorithms in support of operational numerical weather prediction, IEEE Transactions on Geoscience Remote Sensing of Environment, 41, 379-389, doi: 10.1109/TGRS.2002.808307, 2003.

Gunson, M., Farmer, C. B., Norton, R., Zander, R., Rinsland, C. P., Shaw, J., and Gao, B. C.: Measurements of CH4, N2O, CO, H2O, and O3 in the middle atmosphere by the Atmospheric Trace Molecule Spectroscopy Experiment on Spacelab 3, J.
430     Geophys. Res., 95(D9), 13867–13882, doi:10.1029/JD095iD09p13867, 1990.

Hays, P., and Roble, R. G.: Observation of mesospheric ozone at low latitudes, Planetary Space Science, 21, 273-279, https://doi.org/10.1016/0032-0633(73)90011-1, 1973.

Huang, F. T., Reber, C. A., and Austin, J.: Ozone diurnal variations observed by UARS and their model simulation, J. Geophys. Res., 102(D11), 12971–12985, doi:10.1029/97JD00461, 1997.

435     Huang, F. T., Mayr, H. G., Russell, J. M., Mlynczak, M. G., and Reber, C. A.: Ozone diurnal variations and mean profiles in the mesosphere, lower thermosphere, and stratosphere, based on measurements from SABER on TIMED, J. Geophys. Res., 113, A04307, doi:10.1029/2007JA012739, 2008.

Jiang, Y. B., Froidevaux, L., Lambert, A., Livesey, N. J., Read, W. G., Waters, J. W., Bojkov, B., Leblanc, T., McDermid, I. S., Godin-Beekmann, S., Filipiak, M. J., Harwood, R. S., Fuller, R. A., Daffer, W. H., Drouin, B. J., Cofield, R. E., Cuddy, D.
440     T., Jarnot, R. F., Knosp, B. W., Perun, V. S., Schwartz, M. J., Snyder, W. V., Stek, P. C., Thurstans, R. P., Wagner, P. A., Allaart, M., Andersen, S. B., Bodeker, G., Calpini, B., Claude, H., Coetzee, G., Davies, J., De Backer, H., Dier, H., Fujiwara, M., Johnson, B., Kelder, H., Leme, N. P., König-Langlo, G., Kyro, E., Laneve, G., Fook, L. S., Merrill, J., Morris, G., Newchurch, M., Oltmans, S., Parrondos, M. C., Posny, F., Schmidlin, F., Skrivankova, P., Stubi, R., Tarasick, D., Thompson, A., Thouret, V., Viatte, P., Vömel, H., von Der Gathen, P., Yela, M., and Zablocki, G.: Validation of Aura Microwave Limb
445     Sounder Ozone by ozonesonde and lidar measurements, J. Geophys. Res., 112, D24S34, doi:10.1029/2007JD008776. 2007.

Kaufmann, M., Gusev, O. A., Grossmann, K. U., Martin-Torres, F. J., Marsh, D. R., and Kutepov, A. A.: Satellite observations of daytime and nighttime ozone in the mesosphere and lower thermosphere, J. Geophys. Res., 108, 4272, doi:10.1029/2002JD002800, 2003.

Kley, D., Crutzen, P. J., Smit, H. G. J., Vomel, H., Oltmans, S. J., Grassl, H., and Ramanathan, V.: Observations of near-zero
450     ozone concentrations over the convective Pacific: Effects on air chemistry, Science, 274, 230-233, doi:10.1126/science.274.5285.230, 1996.

Koukouli, M. E., Lerot, C., Granville, J., Goutail, F., Lambert, J.-C., Pommereau, J.-P. Balis, D., Zyrichidou, I., Roozendael, M. Van., Coldewey-Egbers, M., Loyola, D., Labow, G., Frith, S., Spurr, R. Zehner, C.: Evaluating a new homogeneous total ozone climate data record from GOME/ERS-2, SCIAMACHY/Envisat, and GOME-2/MetOp-A, J. Geophys. Res. Atmos.,
455     120, 12,296– 12,312, doi:10.1002/2015JD023699, 2015.

Livesey, N., Read, W., Wagner, P., Froidevaux, L., Lambert, A., Manney, G., Pumphrey, H., Santee, M., Schwartz, M., and Wang, S. J. A., JPL publication, USA: Earth Observing System (EOS) Aura Microwave Limb Sounder (MLS) version 4.2 x level 2 data quality and description document, JPL D-33509 rev. A, Jet Propulsion Laboratory, California Institute of Technology, Pasadena, California, 91109-8099, 2015.

460     Livesey, N. J., Filipiak, M. J., Froidevaux, L., Read, W. G., Lambert, A., Santee, M. L., Jiang, J. H., Pumphrey, H. C., Waters, J. W., Cofield, R. E., Cuddy, D. T., Daffer, W. H., Drouin, B. J., Fuller, R. A., Jarnot, R. F., Jiang, Y. B., Knosp, B. W., Li, Q. B., Perun, V. S., Schwartz, M. J., Snyder, W. V., Stek, P. C., Thurstans, R. P., Wagner, P. A., Avery, M., Browell, E. V., Cammas, J.-P., Christensen, L. E., Diskin, G. S., Gao, R.-S., Jost, H.-J., Loewenstein, M., Lopez, J. D., Nedelec, P., Osterman, G. B., Sachse, G. W., and Webster, C. R.: Validation of Aura Microwave Limb Sounder O3 and CO observations in the upper
465     troposphere and lower stratosphere, J. Geophys. Res, 113, doi:10.1029/2007jd008805, 2008.

London , J.: Radiative energy sources and sinks in the stratosphere and mesosphere, Atmospheric Ozone and its Variation and Human Influences, 703, 1980.

Marsh, D. R., Skinner, W. R., Marshall, A. R., Hays, P. B., Ortland, D. A., and Yee, J. H.: High Resolution Doppler Imager observations of ozone in the mesosphere and lower thermosphere, J. Geophys. Res., 107(D19), 4390, doi:10.1029/2001JD001505, 2002.

Masiello, G., Serio, C., Venafra, S., DeFeis, I., and Borbas, E. E.: Diurnal variation in Sahara desert sand emissivity during the dry season from IASI observations, *J. Geophys. Res. Atmos.*, 119, 1626– 1638, doi:10.1002/jgrd.50863, 2014.

Mlynczak, M. G., and Drayson, S. R.: Calculation of infrared limb emission by ozone in the terrestrial middle atmosphere: 1. Source functions, J. Geophys. Res., 95( D10), 16497– 16511, doi:10.1029/JD095iD10p16497, 1990.

Nalli, N. R., Gambacorta, A., Liu, Q., Tan, C., Iturbide-Sanchez, F., Barnet, C. D., Joseph, E., Morris, V. R., Oyola, M. and Smith, J. W.: Validation of Atmospheric Profile Retrievals from the SNPP NOAA-Unique Combined Atmospheric Processing System. Part 2: Ozone, IEEE Trans. Geosci. Remote Sens., 56(1), 598–607, doi:10.1109/TGRS.2017.2762600, 2018.

Noel, V., Chepfer, H., Chiriaco, M., and Yorks, J.: The diurnal cycle of cloud profiles over land and ocean between 51° S and 51° N, seen by the CATS spaceborne lidar from the International Space Station, Atmos. Chem. Phys., 18, 9457–9473, https://doi.org/10.5194/acp-18-9457-2018, 2018.

Olsen, E., Fetzer, E., Hulley, G., Kalmus, P., Manning, E., and Wong, S.: AIRS Version 6 Release Level 2 Product User Guide, Jet Propulsion Laboratory, 2017.

Pallister, R. C., and Tuck, A. F.: The diurnal variation of ozone in the upper stratosphere as a test of photochemical theory, Q J Roy Meteor Soc, 109, 271-284, doi:10.1002/qj.49710946002, 1983.

Parrish, A., Boyd, I. S., Nedoluha, G. E., Bhartia, P. K., Frith, S. M., Kramarova, N. A., Connor, B. J., Bodeker, G. E., Froidevaux, L., Shiotani, M., and Sakazaki, T.: Diurnal variations of stratospheric ozone measured by ground-based microwave remote sensing at the Mauna Loa NDACC site: measurement validation and GEOSCCM model comparison, Atmos. Chem. Phys., 14, 7255-7272, 10.5194/acp-14-7255-2014, 2014.

Petetin, H., Thouret, V., Athier, G., Blot, R., Boulanger, D., Cousin, J.-M., Gaudel, A., Nédélec, P., and Cooper, O.: Diurnal cycle of ozone throughout the troposphere over Frankfurt as measured by MOZAIC-IAGOS commercial aircraft, Elem Sci Anth, 4, 000129, http://doi.org/10.12952/journal.elementa.000129, 2016.

Pittman, J. V., Pan, L. L., Wei, J. C., Irion, F. W., Liu, X., Maddy, E. S., Barnet, C. D., Chance, K., and Gao, R. S.: Evaluation of AIRS, IASI, and OMI ozone profile retrievals in the extratropical tropopause region using in situ aircraft measurements, J. Geophys. Res., 114, D24109, doi:10.1029/2009JD012493, 2009.

Pommier, M., Clerbaux, C., Law, K. S., Ancellet, G., Bernath, P., Coheur, P.-F., Hadji-Lazaro, J., Hurtmans, D., Nédélec, P., Paris, J.-D., Ravetta, F., Ryerson, T. B., Schlager, H., and Weinheimer, A. J.: Analysis of IASI tropospheric $O_3$ data over the Arctic during POLARCAT campaigns in 2008, Atmos. Chem. Phys., 12, 7371–7389, https://doi.org/10.5194/acp-12-7371-2012, 2012.

Prather, M. J.: Ozone in the upper stratosphere and mesosphere, J. Geophys. Res., 86(C6), 5325–5338, doi:10.1029/JC086iC06p05325, 1981.

Rajab, J. M., Lim, H., and MatJafri, M.: Monthly distribution of diurnal total column ozone based on the 2011 satellite data in Peninsular Malaysia, The Egyptian Journal of Remote Sensing Space Science, 16, 103-109, https://doi.org/10.1016/j.ejrs.2013.04.003, 2013.

Read, K. A., Mahajan, A. S., Carpenter, L. J., Evans, M. J., Faria, B. V. E., Heard, D. E., Hopkins, J. R., Lee, J. D., Moller, S. J., Lewis, A. C., Mendes, L., McQuaid, J. B., Oetjen, H., Saiz-Lopez, A., Pilling, M. J., and Plane, J. M. C.: Extensive halogen-mediated ozone destruction over the tropical Atlantic Ocean, Nature, 453, 1232-1235, https://doi.org/10.1038/nature07035, 2008.

Rex, M., Wohltmann, I., Ridder, T., Lehmann, R., Rosenlof, K., Wennberg, P., Weisenstein, D., Notholt, J., Krüger, K., Mohr, V., and Tegtmeier, S.: A tropical West Pacific OH minimum and implications for stratospheric composition, Atmos. Chem. Phys., 14, 4827–4841, https://doi.org/10.5194/acp-14-4827-2014, 2014.

Sakazaki, T., Fujiwara, M., Mitsuda, C., Imai, K., Manago, N., Naito, Y., Nakamura, T., Akiyoshi, H., Kinnison, D., Sano, T., Suzuki, M., and Shiotani, M.: Diurnal ozone variations in the stratosphere revealed in observations from the Superconducting Submillimeter-Wave Limb-Emission Sounder (SMILES) on board the International Space Station (ISS), J. Geophys. Res. Atmos., 118, 2991– 3006, doi:10.1002/jgrd.50220, 2013.

515 Schanz, A., Hocke, K., and Kämpfer, N.: Daily ozone cycle in the stratosphere: global, regional and seasonal behaviour modelled with the Whole Atmosphere Community Climate Model, Atmos. Chem. Phys., 14, 7645–7663, https://doi.org/10.5194/acp-14-7645-2014, 2014.

Seemann, S. W., Borbas, E. E., Knuteson, R. O., Stephenson, G. R., and Huang, H.-L.: Development of a global infrared land surface emissivity database for application to clear sky sounding retrievals from multispectral satellite radiance measurements, 520 J. Appl. Meteor. Climatol., 47, 108–123, https://doi.org/10.1175/2007JAMC1590.1, 2008.

Simpson, D., Arneth, A., Mills, G., Solberg, S., and Uddling, J.: Ozone - the persistent menace: interactions with the N cycle and climate change, Curr Opin Env Sust, 9-10, 9-19, https://doi.org/10.1016/j.cosust.2014.07.008, 2014.

Smith, A. K., and Marsh, D. R.: Processes that account for the ozone maximum at the mesopause, J. Geophys. Res., 110, D23305, doi:10.1029/2005JD006298, 2005.

525 Smith, A. K., Lopez-Puertas, M., Funke, B., Garcia-Comas, M., Mlynczak, M. G., and Holt, L. A.: Nighttime ozone variability in the high latitude winter mesosphere, J. Geophys. Res. Atmos., 119, 13,547– 13,564, doi:10.1002/2014JD021987, 2014.

Smith, N. and Barnet, C. D.: Uncertainty Characterization and Propagation in the Community Long-Term Infrared Microwave Combined Atmospheric Product System (CLIMCAPS), Remote Sens., 11(10), 1227, doi:10.3390/rs11101227, 2019.

Smith, N. and Barnet, C. D.: CLIMCAPS observing capability for temperature, moisture, and trace gases from AIRS/AMSU 530 and CrIS/ATMS, Atmospheric Meas. Tech., 13(8), 4437–4459, doi:10.5194/amt-13-4437-2020, 2020.

Strode, S. A., Ziemke, J. R., Oman, L. D., Lamsal, L. N., Olsen, M. A., and Liu, J.: Global changes in the diurnal cycle of surface ozone, Atmos Environ, 199, 323-333, https://doi.org/10.1016/j.atmosenv.2018.11.028, 2019.

Susskind, J., Barnet, C. D. and Blaisdell, J. M.: Retrieval of atmospheric and surface parameters from AIRS/AMSU/HSB data in the presence of clouds, IEEE Trans. Geosci. Remote Sens., 41, 390–409, 2003.

535 Susskind, J., Blaisdell, J. M., Iredell, L. and Keita, F.: Improved Temperature Sounding and Quality Control Methodology Using AIRS/AMSU Data: The AIRS Science Team Version 5 Retrieval Algorithm, IEEE Trans. Geosci. Remote Sens., 49(3), 883–907, doi:10.1109/TGRS.2010.2070508, 2011.

Susskind, J., Blaisdell, J. M. and Iredell, L.: Improved methodology for surface and atmospheric soundings, error estimates, and quality control procedures: the atmospheric infrared sounder science team version-6 retrieval algorithm, J. Appl. Remote 540 Sens., 8(1), 084994, doi:10.1117/1.JRS.8.084994, 2014.

Tian, B., Yung, Y. L., Waliser, D. E., Tyranowski, T., Kuai, L., Fetzer, E. J. and Irion, F. W.: Intraseasonal variations of the tropical total ozone and their connection to the Madden-Julian Oscillation: THE MJO IN TROPICAL TOTAL OZONE, Geophys. Res. Lett., 34(8), doi:10.1029/2007GL029451, 2007.

Velders, G. J., Andersen, S. O., Daniel, J. S., Fahey, D. W., and McFarland, M.: The importance of the Montreal Protocol in 545 protecting climate, PNAS, 104, 4814-4819, https://doi.org/10.1073/pnas.0610328104, 2007.

Vogt, R., Sander, R., Von Glasow, R., and Crutzen, P. J.: Iodine chemistry and its role in halogen activation and ozone loss in the marine boundary layer: A model study, J Atmos Chem, 32, 375-395, https://doi.org/10.1023/A:1006179901037, 1999.

von Glasow, R., Sander, R., Bott, A., and Crutzen, P. J.: Modeling halogen chemistry in the marine boundary layer 1. Cloud-free MBL, J. Geophys. Res., 107(D17), 4341, doi:10.1029/2001JD000942, 2002.

550 von Glasow, R., von Kuhlmann, R., Lawrence, M. G., Platt, U., and Crutzen, P. J.: Impact of reactive bromine chemistry in the troposphere, Atmos. Chem. Phys., 4, 2481–2497, https://doi.org/10.5194/acp-4-2481-2004, 2004.

Wang, H., Chai, S., Tang, X., Zhou, B., Bian, J., Vömel, H., Yu, K., and Wang, W.: Verification of satellite ozone/temperature profile products and ozone effective height/temperature over Kunming, China, Science of The Total Environment, 661, 35-47, https://doi.org/10.1016/j.scitotenv.2019.01.145, 2019.

555    Waters, J. W., Froidevaux, L., Harwood, R. S., Jarnot, R. F., Pickett, H. M., Read, W. G., Siegel, P. H., Cofield, R. E., Filipiak, M. J., and Flower, D. A.: The earth observing system microwave limb sounder (EOS MLS) on the Aura satellite, IEEE Transactions on Geoscience Remote Sensing, 44, 1075-1092, doi: 10.1109/TGRS.2006.873771, 2006.

Weeks, L., Good, R., Randhawa, J., and Trinks, H.: Ozone measurements in the stratosphere, mesosphere, and lower thermosphere during Aladdin 74, J. Geophys. Res., 83( A3), 978– 982, doi:10.1029/JA083iA03p00978, 1978.

560    WMO: Scientific Assessment of Ozone Depletion: 2010, Global Ozone Research and Monitoring Project-Report No. 52, Geneva, Switzerland, 516, 2011.

WMO: Scientific Assessment of Ozone Depletion: 2014, World Meteorological Organization, Global Ozone Research and Monitoring Project-Report No. 55, Geneva, Switzerland, 416, 2014.

WMO: Scientific Assessment of Ozone Depletion: 2018, Global Ozone Research and Monitoring Project – Report No. 58,
565    Geneva, Switzerland, 588, 2018.

Yang, X., Cox, R. A., Warwick, N. J., Pyle, J. A., Carver, G. D., O'Connor, F. M., and Savage, N. H.: Tropospheric bromine chemistry and its impacts on ozone: A model study, J. Geophys. Res., 110, D23311, doi:10.1029/2005JD006244, 2005.

Zhou, L., Goldberg, M., Barnet, C., Cheng, Z., Sun, F., Wolf, W., King, T., Liu, X., Sun, H., and Divakarla, M.: Regression of surface spectral emissivity from hyperspectral instruments, IEEE Transactions on Geoscience Remote Sensing of
570    Environment, 46, 328-333, doi: 10.1109/TGRS.2007.912712, 2008.

Zhou, D. K., Larar, A. M., and Liu, X.: MetOp-A/IASI Observed Continental Thermal IR Emissivity Variations, IEEE Journal of Selected Topics in Applied Earth Observations and Remote Sensing, 6, 1156-1162, doi: 10.1109/JSTARS.2013.2238892, 2013.

Zommerfelds, W., Kunzi, K., Summers, M., Bevilacqua, R., Strobel, D., Allen, M., and Sawchuck, W.: Diurnal variations of
575    mesospheric ozone obtained by ground-based microwave radiometry, J. Geophys. Res., 94(D10), 12819–12832, doi:10.1029/JD094iD10p12819, 1989.
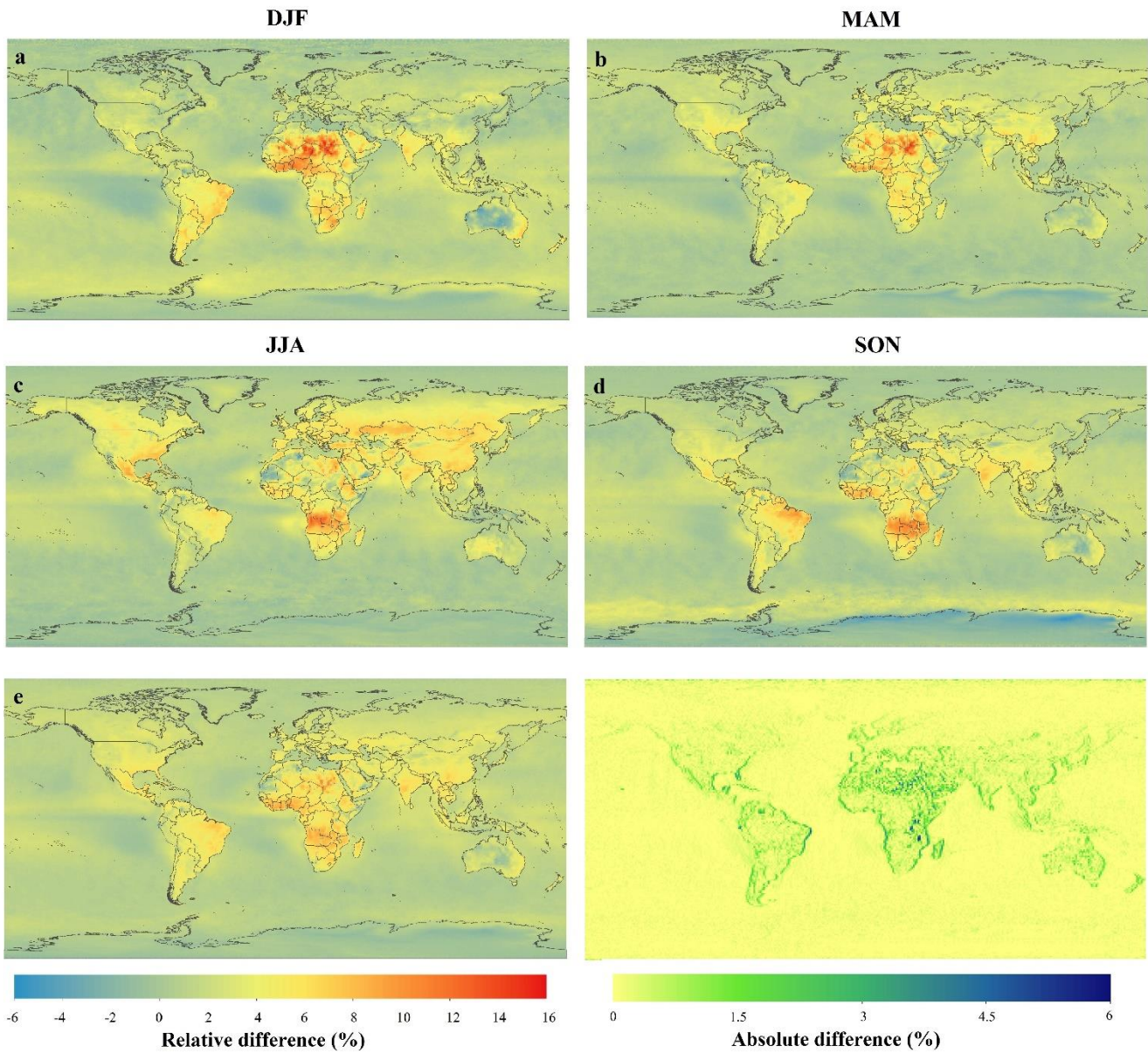
**Figure 1: (a) AIRS TCO averaged day-to-night relative difference for Dec-Jan-Feb during 2003-2018. (b) Mar-Apr-May. (c) Jun-Jul-Aug. (d) Sep-Oct-Nov. (e) AIRS TCO 16-year averaged day-to-night relative difference during 2003-2018. (f) Absolute difference between two adjacent pixels at the same latitude in (e). Note: The relative difference is calculated as: $100 \times$ (daytime - nighttime) / daytime (in percent, %).**
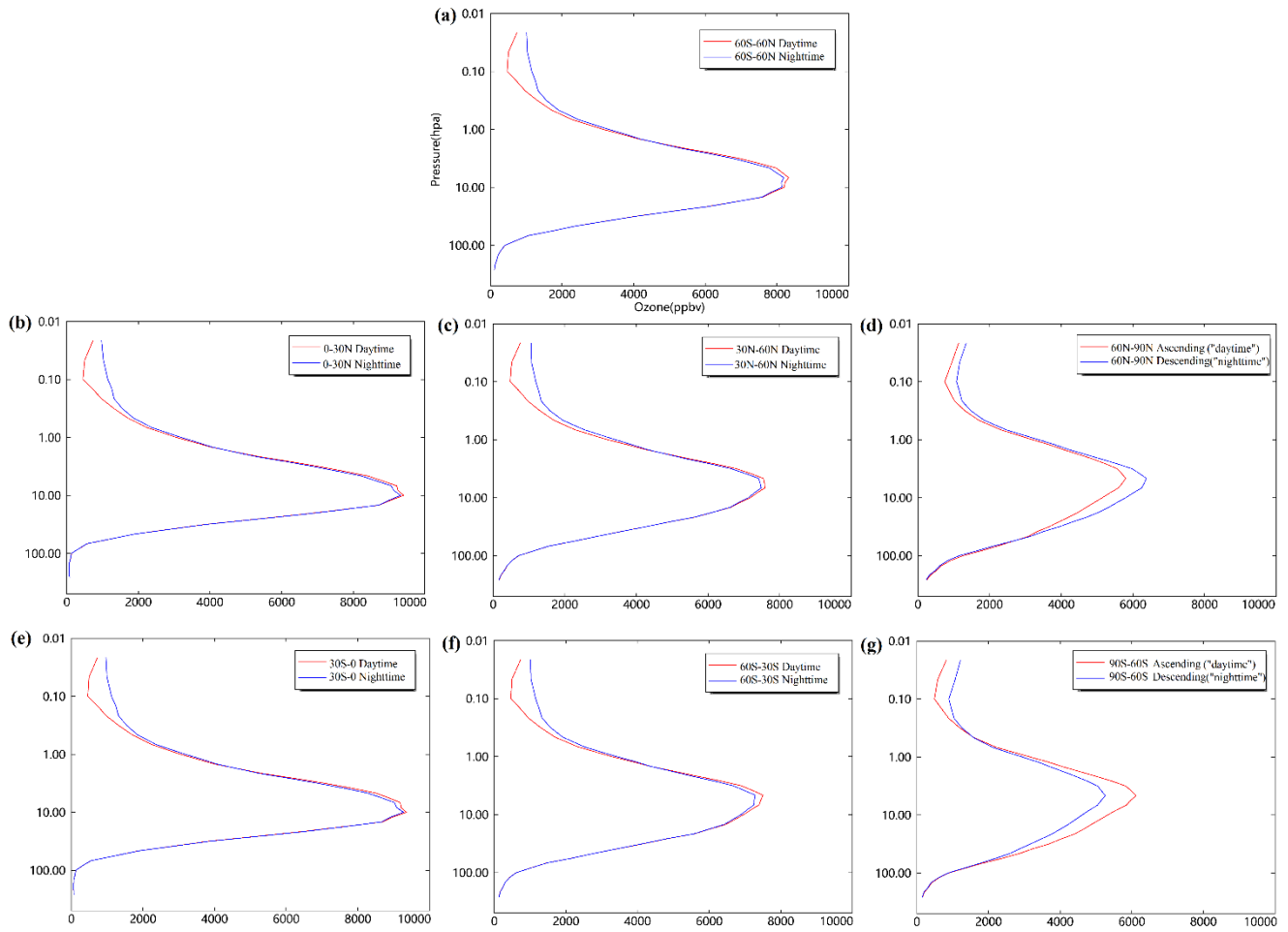
**Figure 2: Averaged MLS ozone profile between 261 hPa and 0.02 hPa per latitude band (30 degree) for 2005-2018. (a) 60 ˚S-60 ˚N. (b) 0-30 ˚N. (c) 30 ˚N-60 ˚N. (d) 60 ˚N-90 ˚N. (e) 30 ˚S-0. (f) 60 ˚S-30 ˚S. (g) 90 ˚S-60 ˚S.**
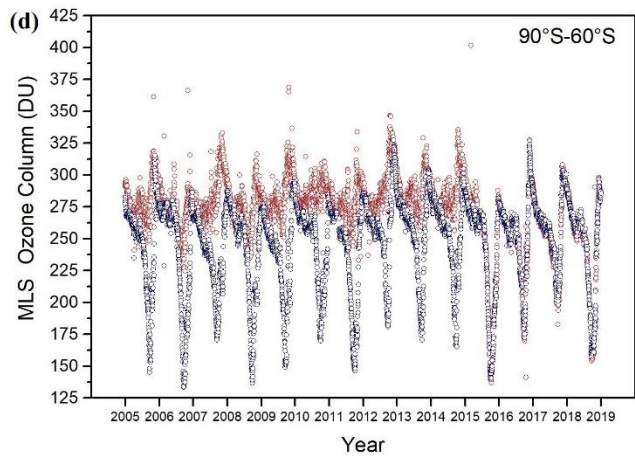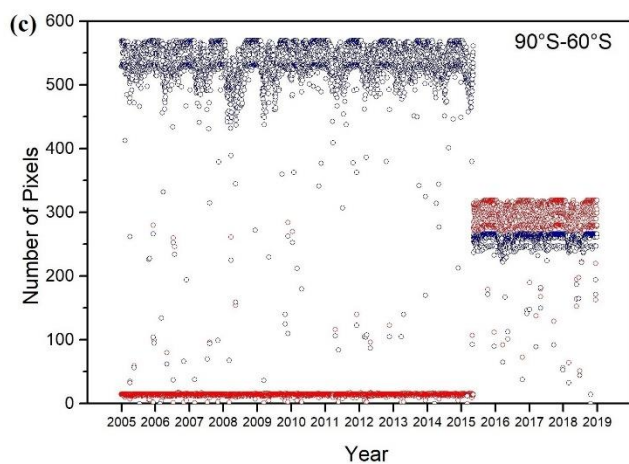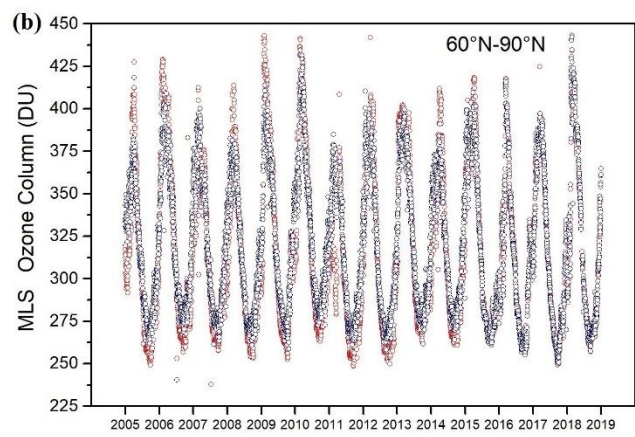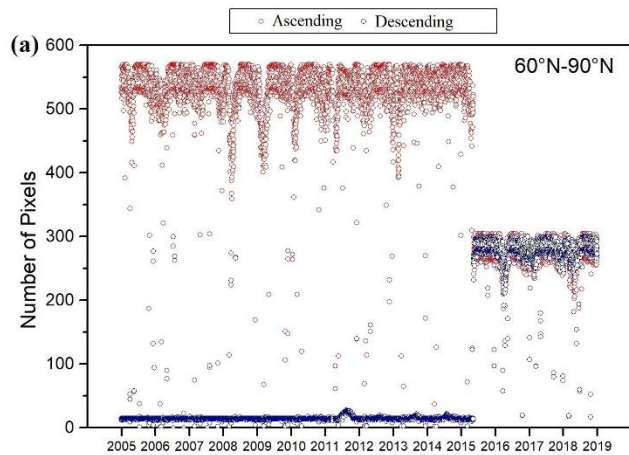
585

**Figure 3: (a) Time series of daily number of Ascending ("daytime") and Descending ("nighttime") pixels in 60 ̊N-90 ̊N. (b) Time series of daily average Ascending and Descending MLS SCO in 60 ̊N-90 ̊N. (c) Same as (a), but in 90 ̊S-60 ̊S. (d) Same as (b), but in 90 ̊S-60 ̊S.**
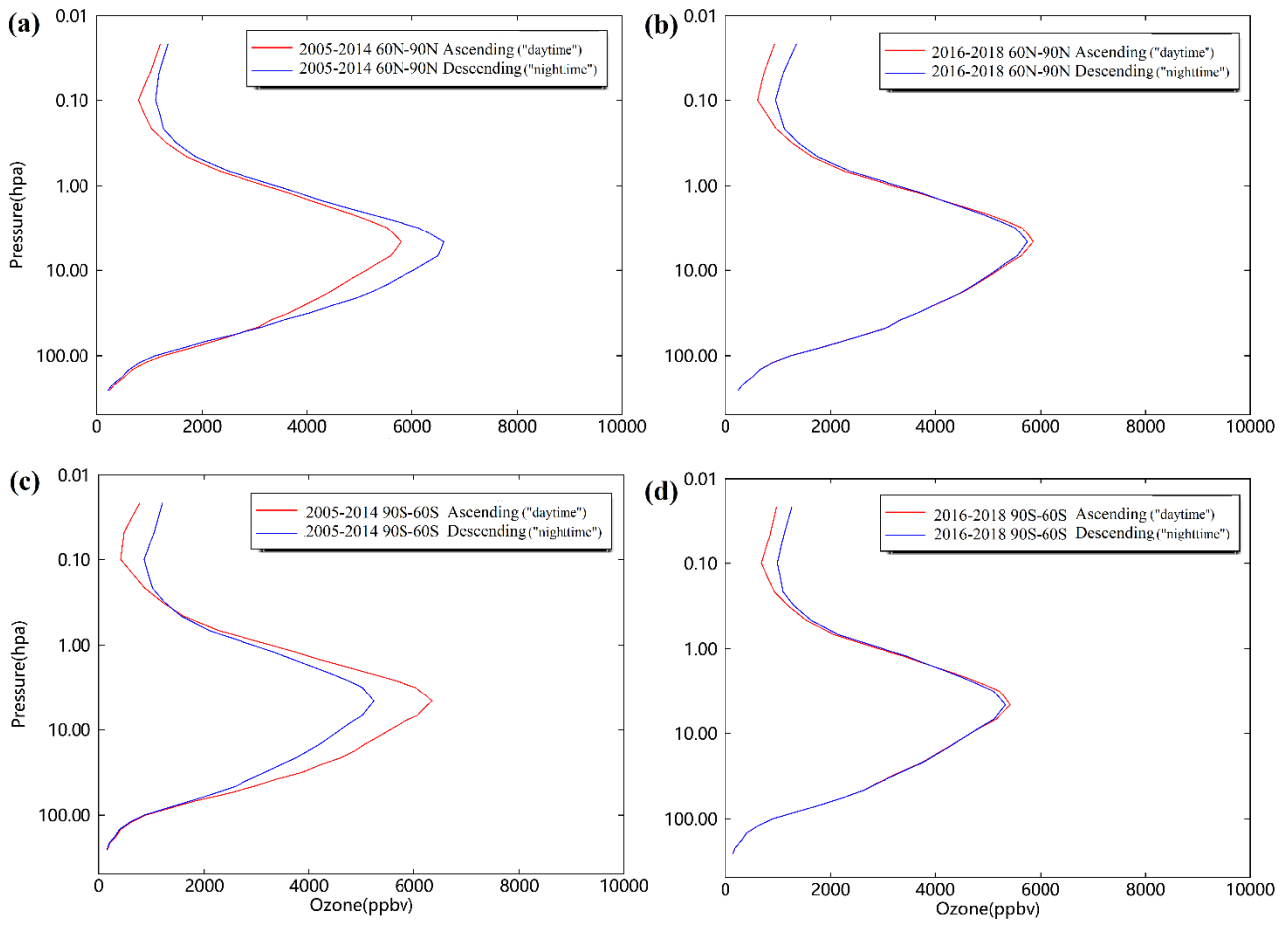
590    **Figure 4: (a) Averaged MLS ozone profile between 261 hPa and 0.02 hPa for 2005-2014 in 60 ̊N-90 ̊N. (b) Averaged MLS ozone profile between 261 hPa and 0.02 hPa for 2016-2018 in 60 ̊N-90 ̊N. (c) Same as (a), but in 90 ̊S-60 ̊S. (d) Same as (b), but in 90 ̊S-60 ̊S.**
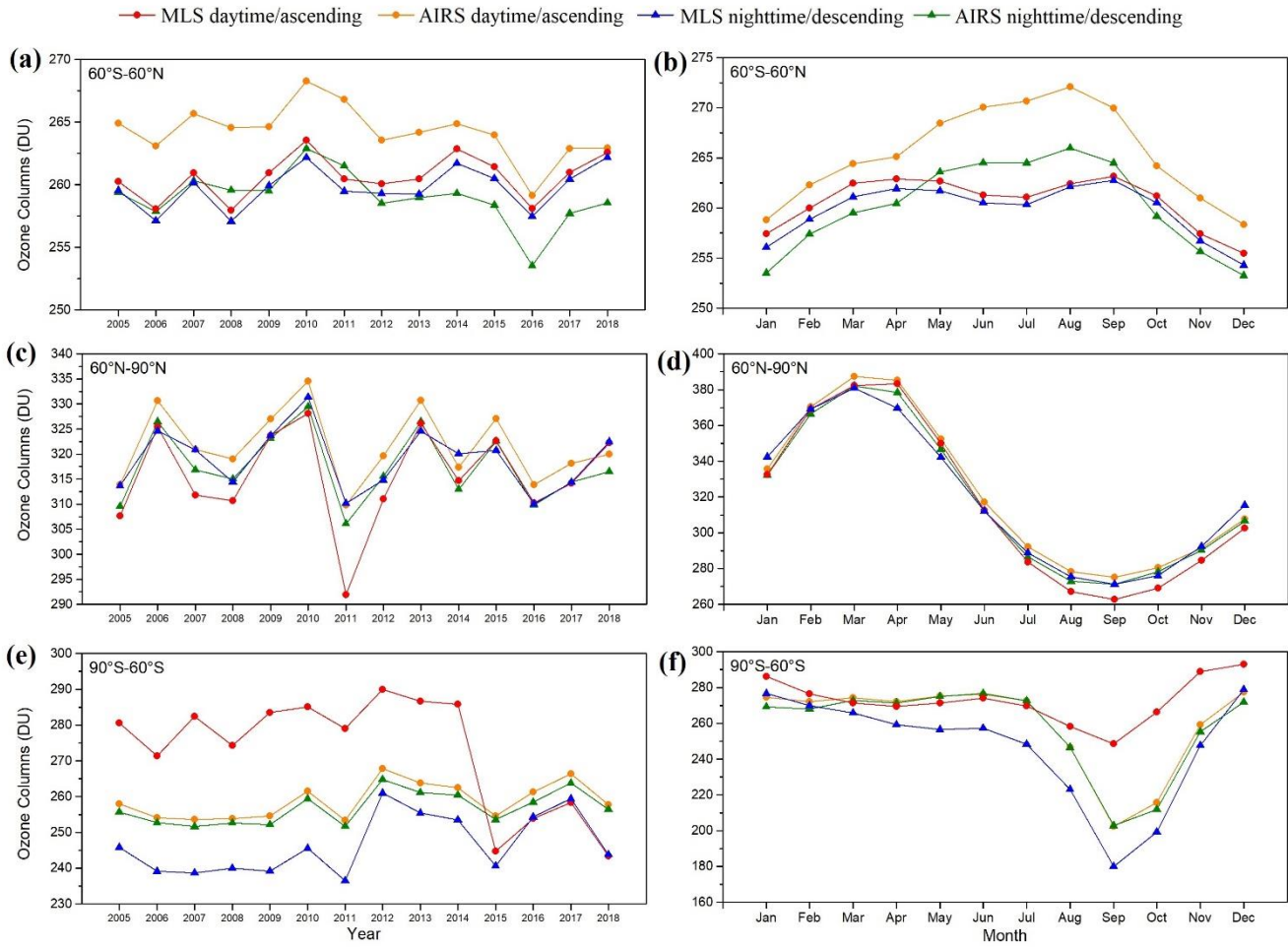
**Figure 5: Yearly and monthly averaged AIRS SCO and MLS SCO for 2005-2018. AIRS SCOs are calculated from 250 hPa to 1 hPa.**

595
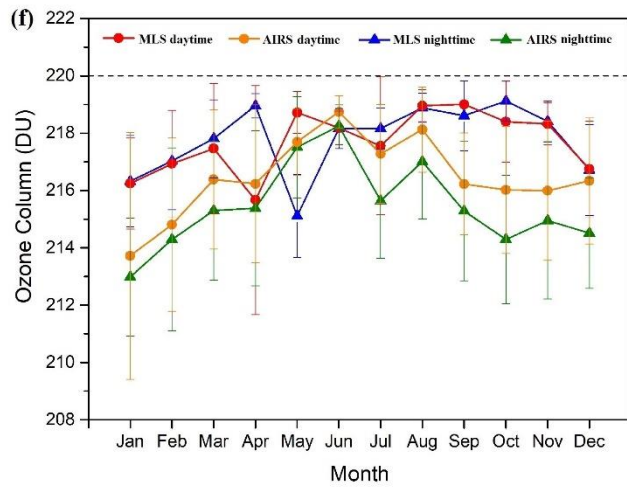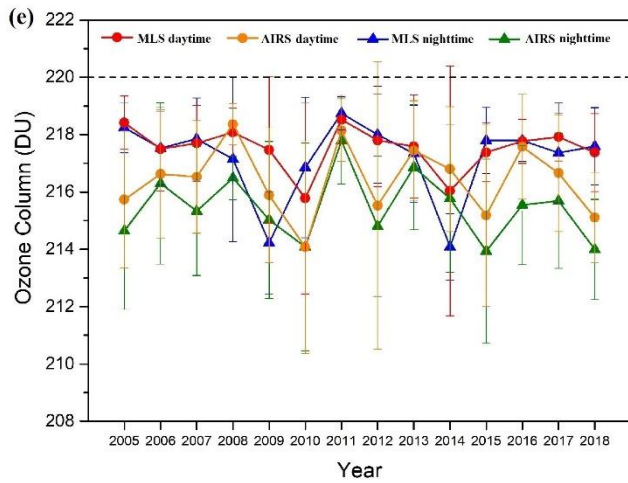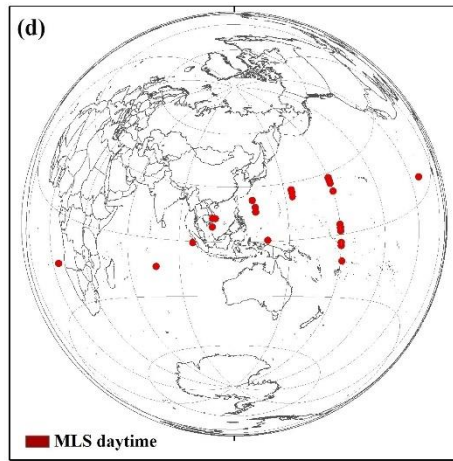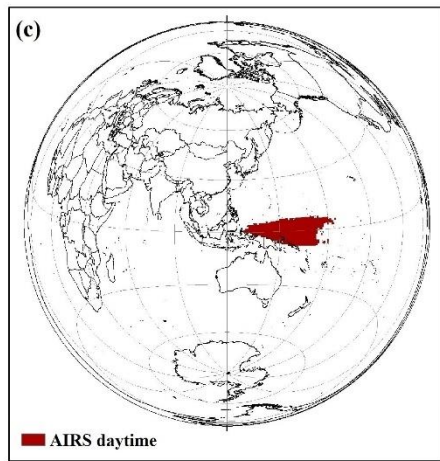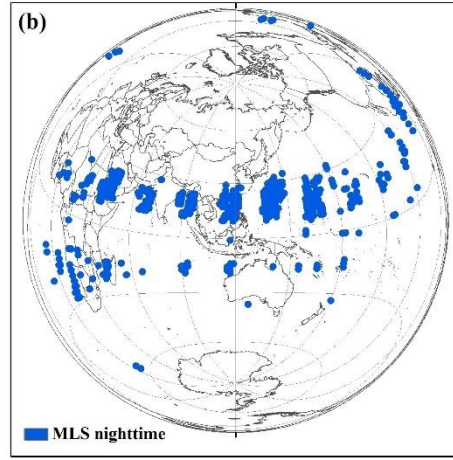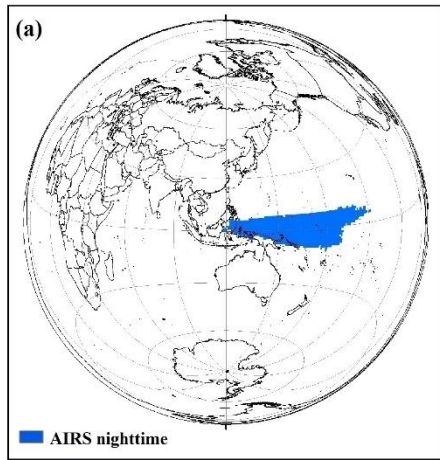
**Figure 6: Spatial and temporal distribution of the low ozone. (a) Location (composite pixel) of the yearly nighttime low ozone from 2005 to 2018 for AIRS TCO. (b) Same as a but for MLS SCO. (c) Location (composite pixel) of the yearly daytime low ozone from 2005 to 2018 for AIRS TCO. (d) Same as c but for MLS SCO. (e) Yearly averaged AIRS TCO and MLS SCO of the low ozone regions for 2005-2018. (f) Monthly averaged AIRS TCO and MLS SCO of the low ozone regions for 2005-2018. Uncertainties represent the standard deviation of the measured values.**

600